Integrated approach using multi-platform sensors for enhanced high-resolution daily ice cover product

George Bonev[a,b], Irina Gladkova*[b], Michael Grossberg[b] , Peter Romanov[b], Sean Helfrich[c,d]

[a] Graduate Center, City University of New York, 365 5th Ave,New York, NY 10016;
[b] The City College of New York, NOAA/CREST, 138th at Convent Ave, New York, NY 10031;
[c] U.S. National Ice Center, Suitland, 4231 Suitland Rd, Suitland, MD 20746;
[d] NOAA/NESDIS,5830 University Research Ct, College Park, MD 20740;

ABSTRACT

The ultimate objective of this work is to improve characterization of the ice cover distribution in the polar areas, to improve sea ice mapping and to develop a new automated real-time high spatial resolution multi-sensor ice extent and ice edge product for use in operational applications. Despite a large number of currently available automated satellite-based sea ice extent datasets, analysts at the National Ice Center tend to rely on original satellite imagery (provided by satellite optical, passive microwave and active microwave sensors) mainly because the automated products derived from satellite optical data have gaps in the area coverage due to clouds and darkness, passive microwave products have poor spatial resolution, automated ice identifications based on radar data are not quite reliable due to a considerable difficulty in discriminating between the ice cover and rough ice-free ocean surface due to winds. We have developed a multi-sensor algorithm that first extracts maximum information on the sea ice cover from imaging instruments VIIRS and MODIS, including regions covered by thin, semitransparent clouds, then supplements the output by the microwave measurements and finally aggregates the results into a cloud gap free daily product. This ability to identify ice cover underneath thin clouds, which is usually masked out by traditional cloud detection algorithms, allows for expansion of the effective coverage of the sea ice maps and thus more accurate and detailed delineation of the ice edge. We have also developed a web-based monitoring system that allows comparison of our daily ice extent product with the several other independent operational daily products.

Keywords: sea-ice extent; multi-sensor fusion; visible, infrared, passive microwave instruments; Arctic; Antarctic; MODIS; VIIRS; AMSR-2;

1. INTRODUCTION

Sea ice cover is both an important indicator and a critical factor in Earth's climate and weather system. The overall distribution of sea ice in the Arctic and Antarctic regions has a significant impact on water management, transportation, weather forecasting, and climate change studies. It affects atmosphere-ocean energy exchange by modulating the physical and optical properties of the ocean surface [1]. The character and distribution of sea ice affects the thermohaline structure and the fresh water balance of the ocean. Thus in understanding both ocean and atmosphere it is critical to monitor ice cover distribution, seasonal variability and long-term trends. These trends in the polar region may be studied through parameters such as the position of the sea ice front, total ice extent, ice concentration and thickness [2-7]. These parameters are widely viewed as major indicators of climate variability and change. In addition to their use for understanding and monitoring the climate, sea ice extent and concentration are key inputs to numerical weather prediction (NWP) models operated by National Centers for Environmental Prediction (NCEP) of NOAA National Weather Service (NWS).

Despite several currently available automated satellite-based ice cover datasets, analysts at National Ice Center (NIC) tend to rely on original satellite imagery from optical, passive microwave and active microwave sensors in their daily interactive analysis. This is primarily due to the fact that different instruments have different strengths and weaknesses

Earth Observing Systems XXI, edited by James J. Butler, Xiaoxiong (Jack) Xiong, Xingfa Gu, Proc. of SPIE
Vol. 9972, 997213 · © 2016 SPIE · CCC code: 0277-786X/16/$18 · doi: 10.1117/12.2244976

with respect to ice retrievals and there is no automated algorithm compatible with interactive sea ice analysis that integrates the observations from instruments of various types, which fully preserves the complementary information available from each instrument type.

Given the limitations of optical and microwave instruments, developing ice products that integrate sensors is an important area of open research [8]. Currently the most widely used multisensor ice product is produced by the Interactive Multisensor Snow and Ice Mapping System (IMS) operated by the National Ice Center (NIC) [9 - 11]. IMS is operated by trained analysts who produce a daily digital product utilizing Geographic Information System technology and incorporating a variety of, and an ongoing expansion of, technological capabilities as well as sources of information. IMS produces estimates of snow and sea ice extent across the globe every day, regardless of the presence of clouds. This is possible primarily for two reasons. First, analysts supplement visible and near infrared imagery with many other sources of information such as passive microwave and active radar data. Second, because IMS analysts use a temporal sequence of images over recent days, they can integrate of information from both spatial and temporal perspectives. Thus, a key feature of the IMS product is that human judgment as to which data sources are most reliable in different conditions and regions, and as to the final evaluation of where sea ice is, remains an integral part of the process, and one of the strengths of the IMS product. However, manual sea ice mapping drawn by humans, is a subjective, labor intensive and time consuming procedure, that is not easily scalable as satellite resolution increases. Automated algorithm would unequivocally facilitate the work of human ice analysts and would result in more accurate ice products including ice extent, edge and type.

We have developed and evaluated an automated algorithm, MISIC, which capable of using imager and microwave data from multiple instruments (MODIS, VIIRS, and AMSER-2) to estimate sea ice cover. The most distinctive feature of our approach is that we can use high-resolution imager data partially obscured by (thin) clouds to do open water versus sea ice classification. No other algorithm has this capability. When thin clouds are present, the MISIC single-pass enhanced product can combine the high resolution surface features only partially obscured by clouds, with the most recent microwave data, to produce the best current estimate the sea ice on the surface. When the surface covered by thick clouds, the algorithm fills the missing data using cloud penetrating microwave data, at the cost of lower resolution. We have also shown that by combining the single-pass enhanced automated ice mask into a daily product increase the resolution over microwave where surface features were visible, potentially through thin clouds, at some point during the day.

2. TRAINING DATA

We have used in our study, the representative cases annotated by NIC analysts. The representative images over regions of interest were subjectively chosen and annotated by different analysts. Figure 1 shows examples used to develop the algorithm. As can be seen from Figure 1, the image enhancements used by human operators vary from case to case. The annotations indicate where open water is visible both with and without thin clouds. Other annotations also indicate ice with and without thin cloud, as well as thick cloud regions where determination of the surface from reflected light imagery is likely impossible. From examination of the annotated images, we have manually marked up small representative areas near the points annotated with similar visual properties.

Since the goal of the algorithm to identify the surface as ice or water wherever that determination is possible, we have introduced the following 5 classes: 1) confident open water which may be covered by a thin cloud (rendered in blue); 2) water under clouds which is visually identifiable from the natural color imagery (rendered in green); 3) confident sea ice which may have thin cloud (rendered in red); 4) thick cloud (rendered in yellow); and 5) uncertain regions which may include cloud shadows (magenta), mixed or broken ice, leads and polynyas (cyan). We have used this labeled data set for feature selection, ice/water classification algorithm development, ice/water daily composite maps and case-by-case validation.

The traditional automated sea ice extent algorithms usually rely on available cloud mask, which in general is more conservative in identifying clouds than human ice analyst. When the clouds are thin and ice or water is clearly visible, NIC analysts would use that information in their classification of ice extent. A particularly useful false color composition that partially enables such classification can built from the MODIS instrument using derived reflectance from $R_{0.47nm}$

(MODIS band 3), $R_{1.6nm}$ (MODIS band 6), $R_{2.4nm}$ (MODIS band 7) which are usually visualized as RGB respectively. For this 3-6-7 false color RGB, the displayed red channel, corresponding to measurements in visible spectra (band 3), provide a clear distinction between water versus cloud and ice, whereas the IR bands 6 and 7 (green and blue) facilitate ice versus cloud discrimination. In the visible spectral bands cloud and ice appear much brighter then water, while in the IR spectra ice appears much darker than clouds. As a result the 3-6-7 false color image will show ice in bright red (high value only in $R_{0.47nm}$), cloud in white (high values in all three bands) and water will appear dark (low values in all three bands). 3-6-7 False color images corresponding to the selected marked-up examples are shown in Figure 2. The main challenge in visual identification of sea ice is discriminating the water from shadowed regions. The cloud shadow over either sea ice surface or over another cloud is appearing dark and can be easily confused with open water.

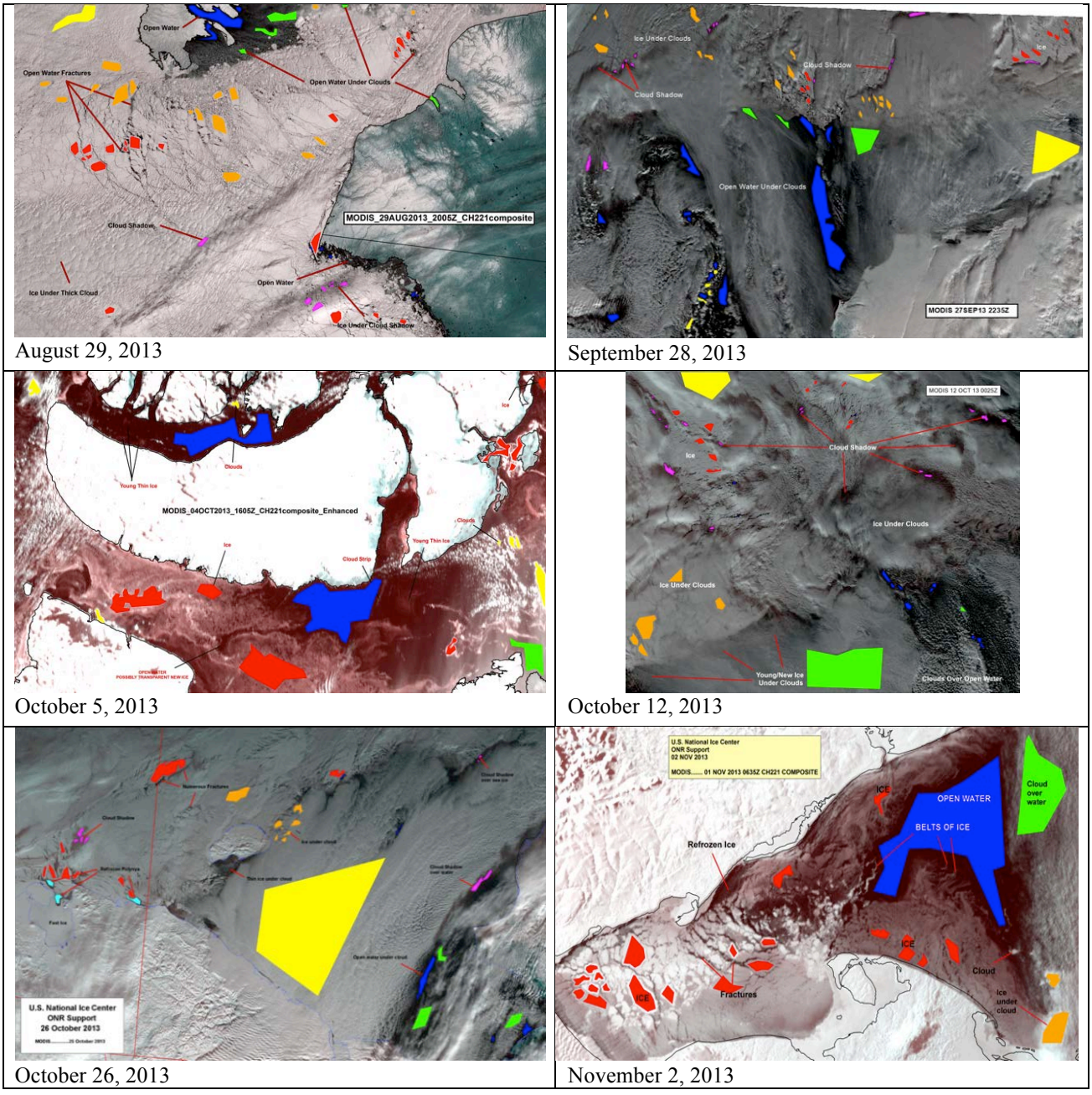

Figure 1: Six representative examples of NIC special support and manual mark-up.

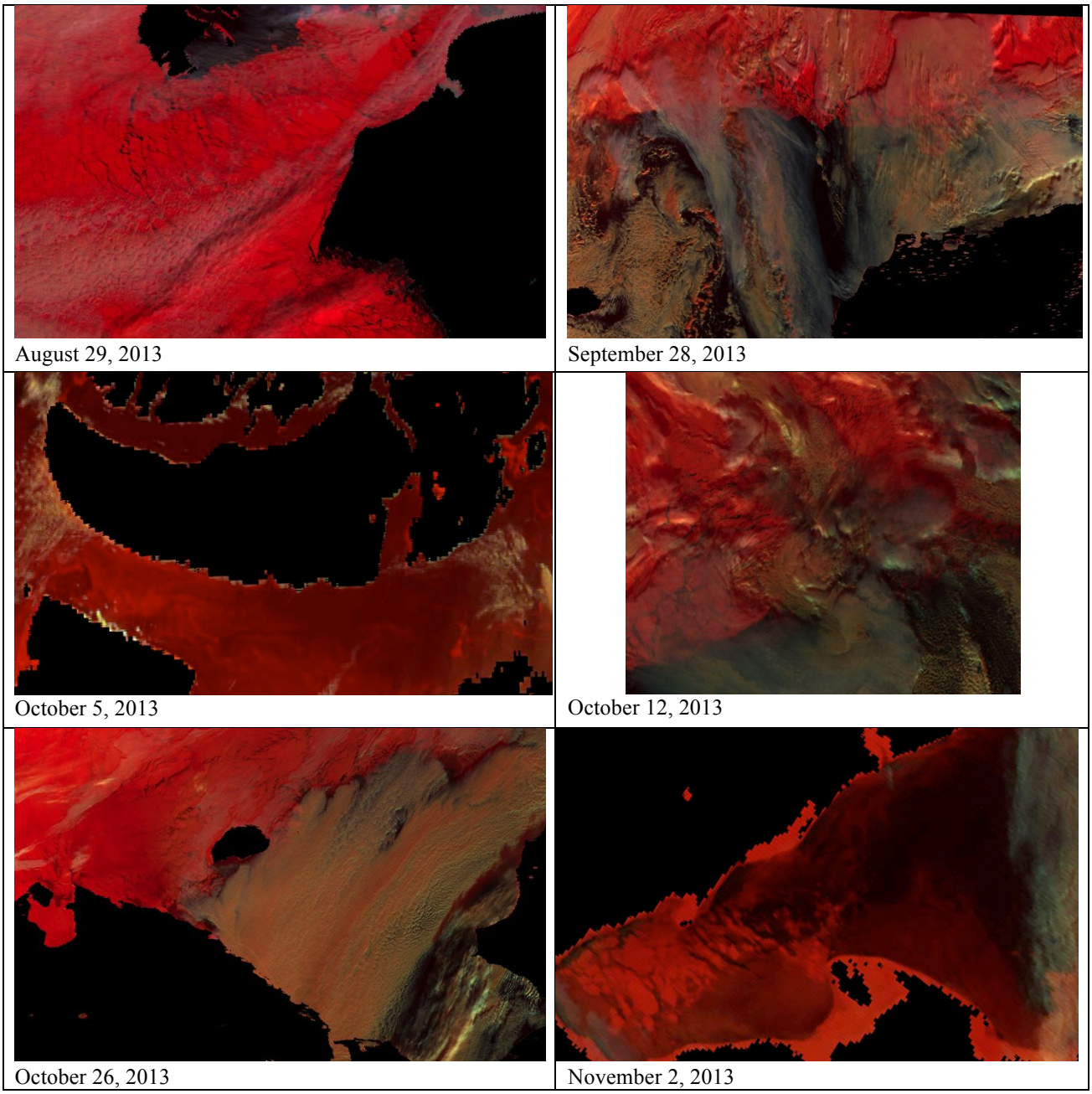

Figure 2: 3-6-7 False color images, corresponding to selected examples shown in Figure 1.

Figure 3 shows 2D scatter plots of band 3 and 6 reflectance values, for all of the manually marked up classes, using the same coloring scheme as in Figure 1. As can be seen in these plots, water, ice and cloud clusters appear to be separable for each individual example. The relative positions of the classes with respect to each other are preserved, with ice (red) on the right, water (blue) in the lower left, and clouds (yellow) at the top of the scatter plots. Clouds over water (green) are falling between water and cloud clusters and clouds over ice (orange) are similarly located on the path from ice to cloud. This suggests using visible bands as the "R" direction of the false color space and bands 6 and 7 as "G" direction. Shadows (magenta) are appearing in the middle, sometimes overlapping with ice pixels and sometimes spreading towards the "water domain".

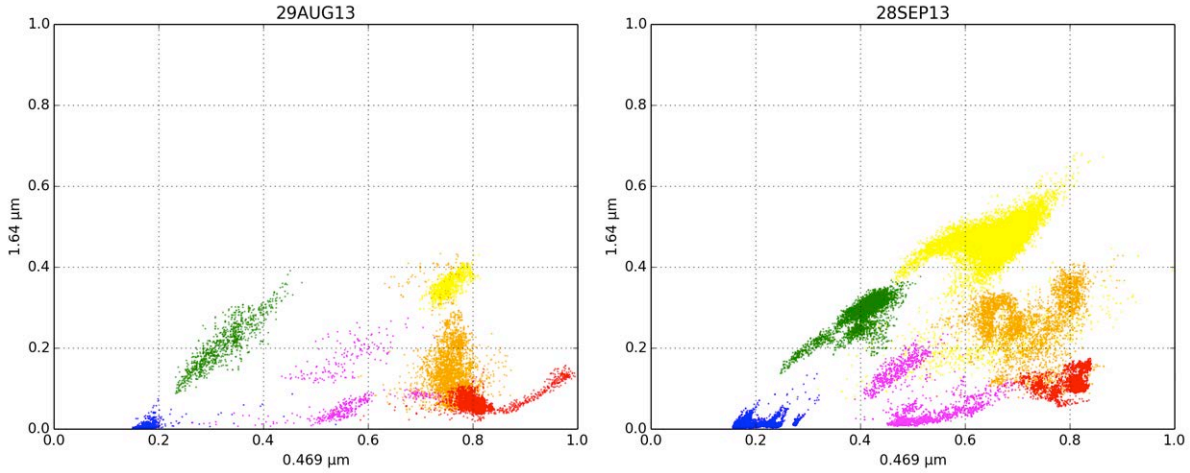

a) 29 Aug 2013

b) 28 Sept 2013

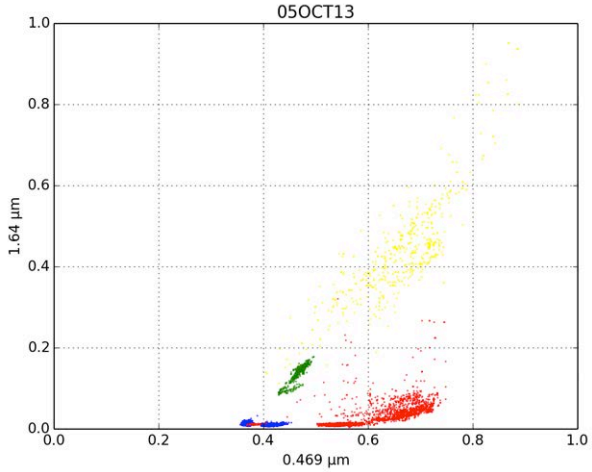

c) 05 Oct 2013

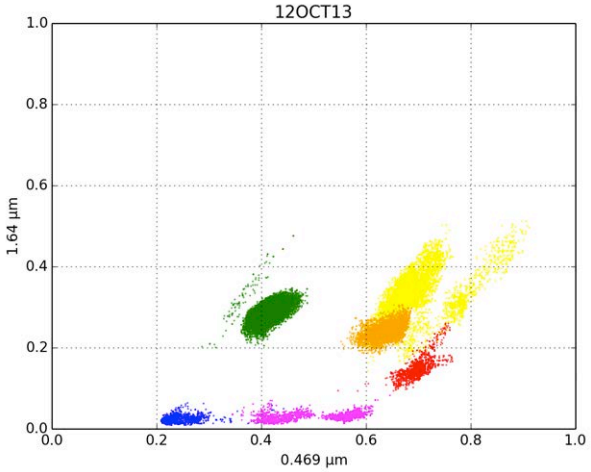

d) 12 Oct 2013

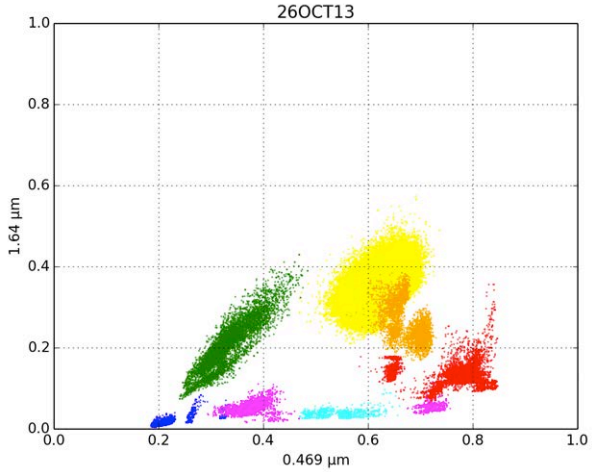

e) 26 Oct 2013

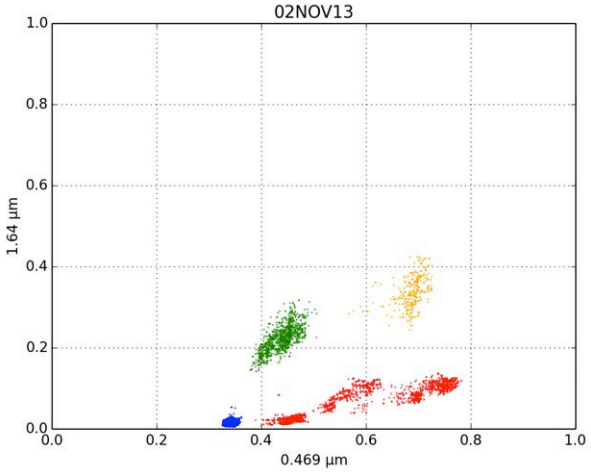

f) 02 Nov 2013

Figure 3: Scatter plots of labeled class data from NIC annotated examples.

We should note at this point that although the relative position of the classes within single case study is the same, there is a significant variation with respect to the position of each class across the different images (cf. Figure 3). This makes it difficult to separate the classes using distance measures from pixels with known classes such as universal thresholds, nearest neighbor methods or queries to Look Up Tables (LUT). These variations are attributed to satellite viewing angle, solar zenith angle, atmospheric conditions, and seasonal cycles. Therefore, the selected features should be at least partially invariant.

We have introduced a novel 3D false color feature space which shares the property the 3-6-7 false color composition that ice is displayed in red. This was achieved utilizing manually labeled satellite imagery (including examples shown in Figures 1-3), by expert analysts from the National Ice Center (NIC). The spectral signatures of each target class were extracted and used to compute coefficients to a logistic function that maps the input albedo into a feature whose value is high for the class it was derived for.

The purpose of this novel feature space is to emphasize the two main classes – the ice class and the water class even if they are partially obscured by clouds. Since the cloud class was of no interest for this study, we call the desired 3D feature space and the corresponding false color composition as Ice-Water (I-W) space and I-W false color image. With "white" allocated for geographically determined land, the color choice for clouds and water classes were considered to be yellow and blue respectively. That choice called for a space with (0,0,1) corner reserved for water (high in blue and low in the other two components), (1,0,0) corner allocated for ice (high in red and low in other components) and (1,1,0) corner reserved for clouds (high in both, red and green; low in blue) as shown in Figure 4a). The 9D space containing reflective, shortwave IR and thermal bands centered around 0.46nm, 0.56nm, 0.65nm, 0.86nm, 1.24nm, 1.6nm, 2.2nm, 11nm and 12nm is projected to 3D color cube, mapping seven types of spectral curves into seven (color-coded) corners of the RGB cube, shown in Figure 4a). Spectral curves over reflective bands corresponding to selected representative water pixels (blue), shadows (black), ice-covered pixels (red), cloudy pixels (green) are shown in Figure 4b).

The I-W false color images, corresponding to the same six selected cases as in Figs 1-3, are shown in Figure 5. The ice is more pronounced then in 3-6-7 False Color images (cf. Fig. 2), especially under thin clouds. The shadowed regions (appearing dark) are also much more separable from open water (blue).

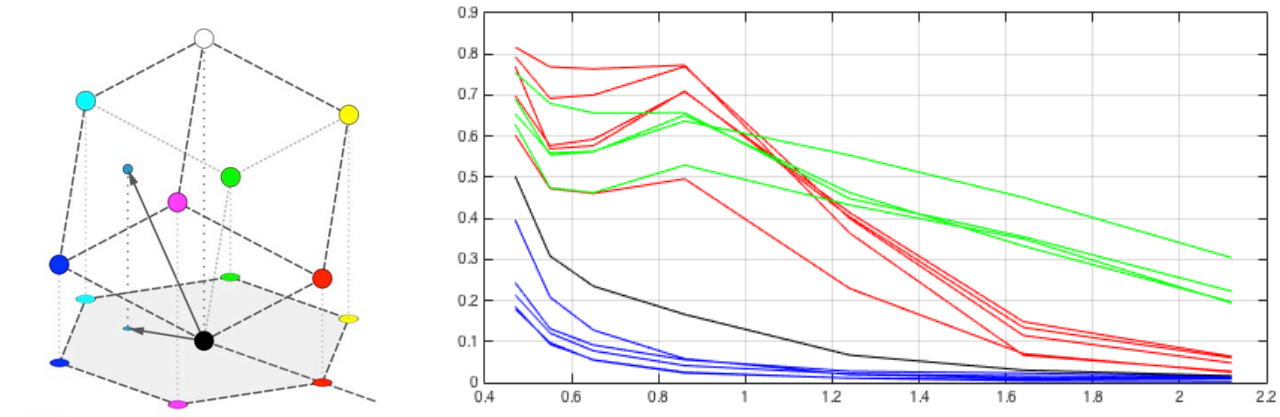

a) b)

Figure 4: a) False color cube with colors corresponding to selected classes: shadows (black), water (blue), thin cloud over water (cyan), ice (red), thin cloud over ice (yellow), cloud (green), thin ice or cold, nearly freezing point water (magenta); **b)** Spectral curves corresponding to selected representative water pixels (blue), shadows (black), ice-covered pixels (red), cloudy pixels (green).

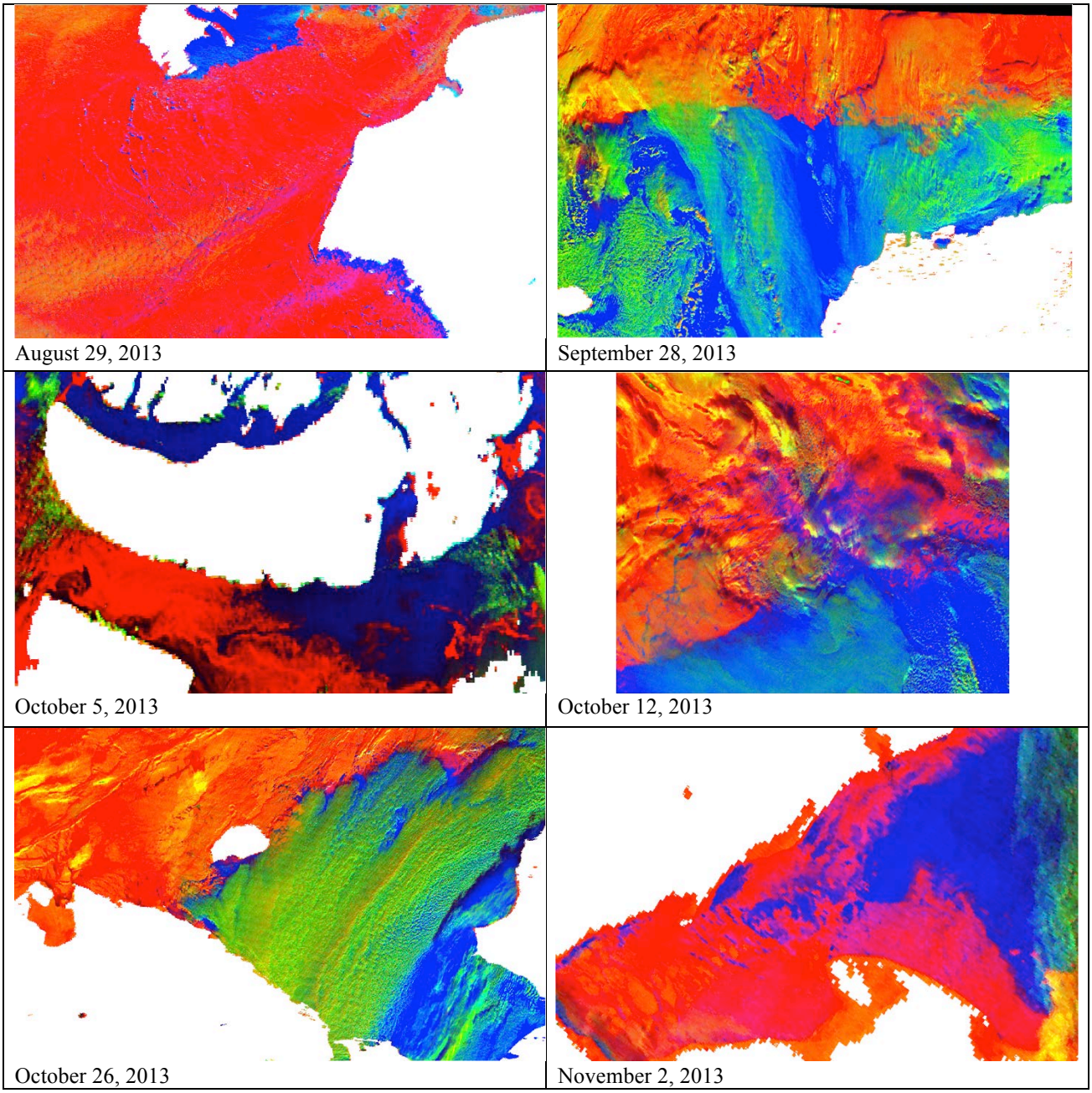

Figure 5: I-W False color for annotated examples shown in Figure 1. The ice is more pronounced then in 3-6-7 False Color images (cf. Fig. 2), especially under thin clouds. The shadowed regions (appearing dark) are also much more separable from open water (blue).

3. ALGORITHM DESCRIPTION

The algorithm first extracts maximum information on the sea ice cover from imaging instruments VIIRS and MODIS, including regions covered by thin, semitransparent clouds using our I-W 3D feature space. This ability to identify ice cover underneath thin clouds, which is usually masked out by traditional cloud detection algorithms, allows for expansion of the effective coverage of the sea ice maps and thus more accurate and detailed delineation of the ice edge. In the next step of our algorithm, the labels obtained from individual imager overpass observations are supplemented by

the microwave measurements, resulting in 5 intermediate classes: sea ice, ice-free water, ice under thick clouds, water under thick clouds and an undetermined class where there is insufficient information. For example, grid cells under cloud near the ice edge, cannot be precisely determined by the lower resolution microwave ice concentration product. The confidently labeled grid cells serve as a training set for a Linear Discriminant Analysis (LDA) classifier in the I-W feature space as well as polarization and gradient ratios of 18 and 36 GHz radiometer channels of the microwave instrument.

The microwave data makes it possible to classify grid cells under thick clouds that cannot be classified using the imager input alone. Although this particular step of the algorithm relies on the classification involving microwave data and therefore results in a somewhat degraded effective spatial resolution of the ice extent, these grid cells have a special "microwave" tag and weighted less in the last step of the algorithm which combines the labels from the individual overpasses in an optimal way into daily ice extent product, resulting in the enhanced, high resolution, gap free ice extent product.

The algorithm relies on re-gridded imager and microwave overpasses for a predetermined geographic region and consists of 3 main steps:

- **Step 1**. Extracts maximum information on the sea ice cover from a single pass of one of the imaging instruments VIIRS and MODIS, including regions covered by thin, semitransparent clouds;
- **Step 2**. Supplements classification by the microwave measurements, resulting in 5 intermediate classes:

    1) ice-free water,
    2) sea ice,
    3) water under thick clouds,
    4) ice under thick clouds,
    5) undetermined class (insufficient information);

- **Step 3**. Generates (per imager overpass) a supervised classifier, using labels from Step A2 as a training set in an experimentally derived feature space constructed from reflective, shortwave IR and thermal bands centered around 0.46nm, 0.64nm, 0.86nm, 1.24nm, 1.6nm, 11nm and 12nm from the imager instrument as well as polarization and gradient ratios of 18 and 36 GHz radiometer channels of the microwave instrument;

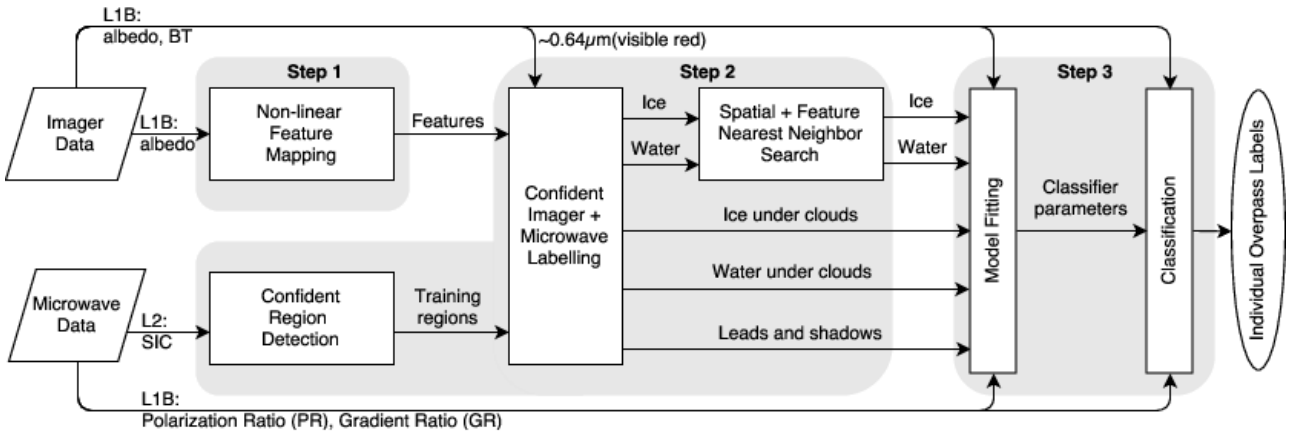

Figure 6. Block diagram of imager overpass classification. Main steps of the algorithm are shaded in light grey as they consist of multiple block elements. The data flow is outlined by the input/output arrows.

The block diagram in Figure 6 shows the main components of the imager overpass labeling procedure. Steps 1-3 are shaded in light grey as they consist of multiple block elements. The first step of the algorithm requires only imager. It relies on our 3D feature color space that suppresses thin clouds and amplifies the discrimination between open water and ice. The 2nd and 3rd steps require data from both types of instruments: imager and microwave, introducing 2 additional

classes – ice under cloud and ice-free water under cloud. During Step 2, the grid cells that are not classified in the previous step due to cloud obstruction of the imager data and are located away from the ice edge or coast line as determined by the microwave sea ice concentration product or land mask, respectively, are classified as "water under cloud" and "ice under cloud" using the microwave sea ice concentration product. This step classifies some cloud covered grid cells, but not all, leaving many grid cells labeled as "to be determined" for Step 3, which takes the already labeled points as a training set and uses them to construct scene-dependent classifier in a feature space that includes both, imager and microwave data, based on which the remaining "to be determined" points are labeled. The intuition is that the previous step outputs examples of grid cells for all classes present in the scene, which allows us to fit a statistical model using Linear Discriminant Analysis (LDA). The inputs to the classifier are the features derived in Step 1, as well as the two normalized difference ratios used in producing the standard level 2 passive microwave ice fraction product, i.e. Polarization Ratio (PR) and Gradient Ratio (GR). This results in a 5-dimensional feature space. Once the model is fit to the training data, it is applied to assign one of the five target classes across the remaining unknown grid cells. The passive microwave inputs are directly used, rather than their derived ice concentration, to preserve as much information as possible for the classification. The final result of this classification is shown in Figure 2(e).

Figure 7 shows few representative overpasses out of 30+ for VIIRS (Suomi NPP) and MODIS (both, Aqua and Terra), acquired on August 6, 2015. Overpasses selected to demonstrate typically challenging cases: thin clouds, shadows, ice floes, low sun angles, etc. The results of classification (Steps 1 -3) corresponding to each overpasses of Figure 7 are shown in Figure 8.

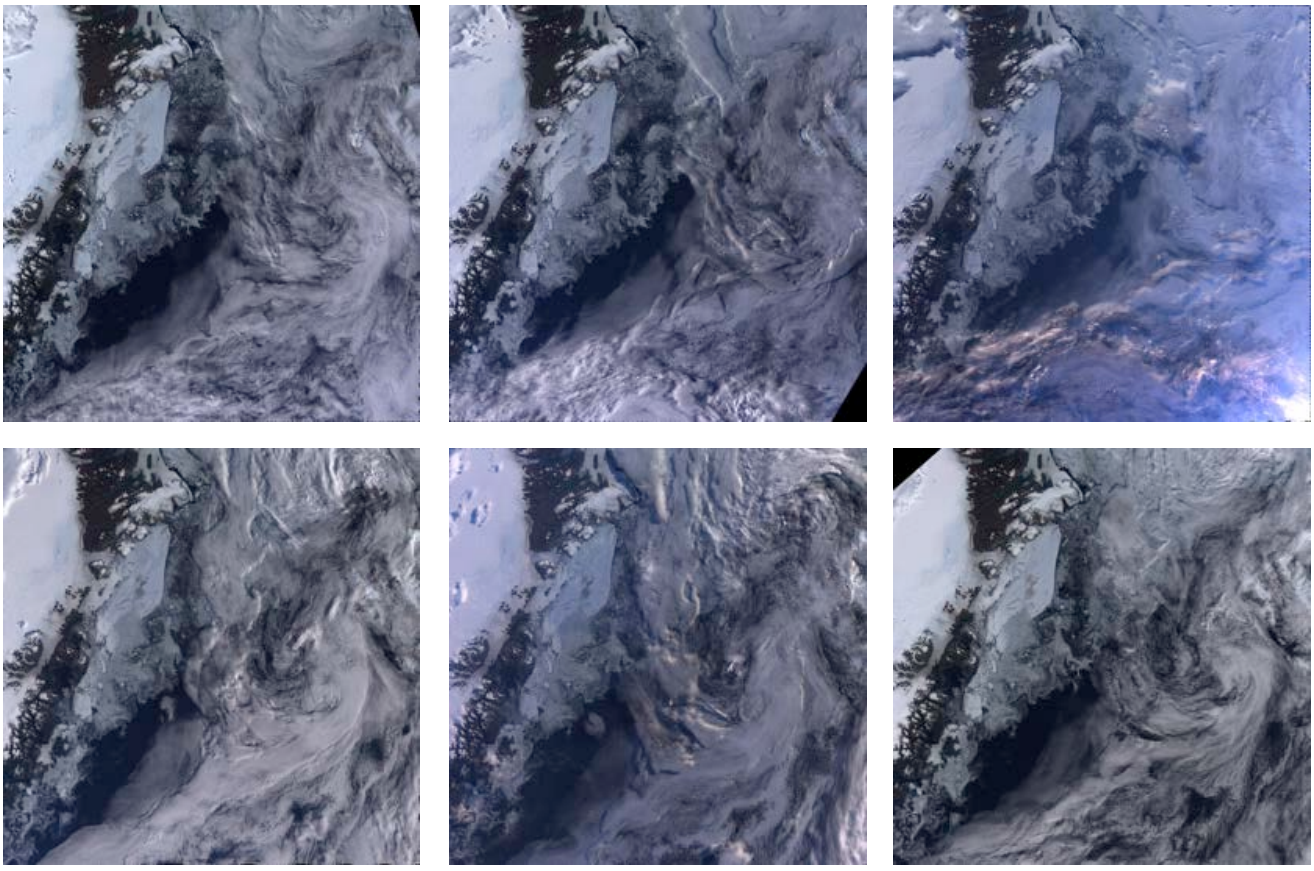

Figure 7. Six representative overpasses out of 30+ combined for VIIRS (Suomi NPP) and MODIS (both Aqua and Terra), acquired on August 6, 2015, showing some challenging cases: thin clouds, shadows, ice floes, low sun angles.

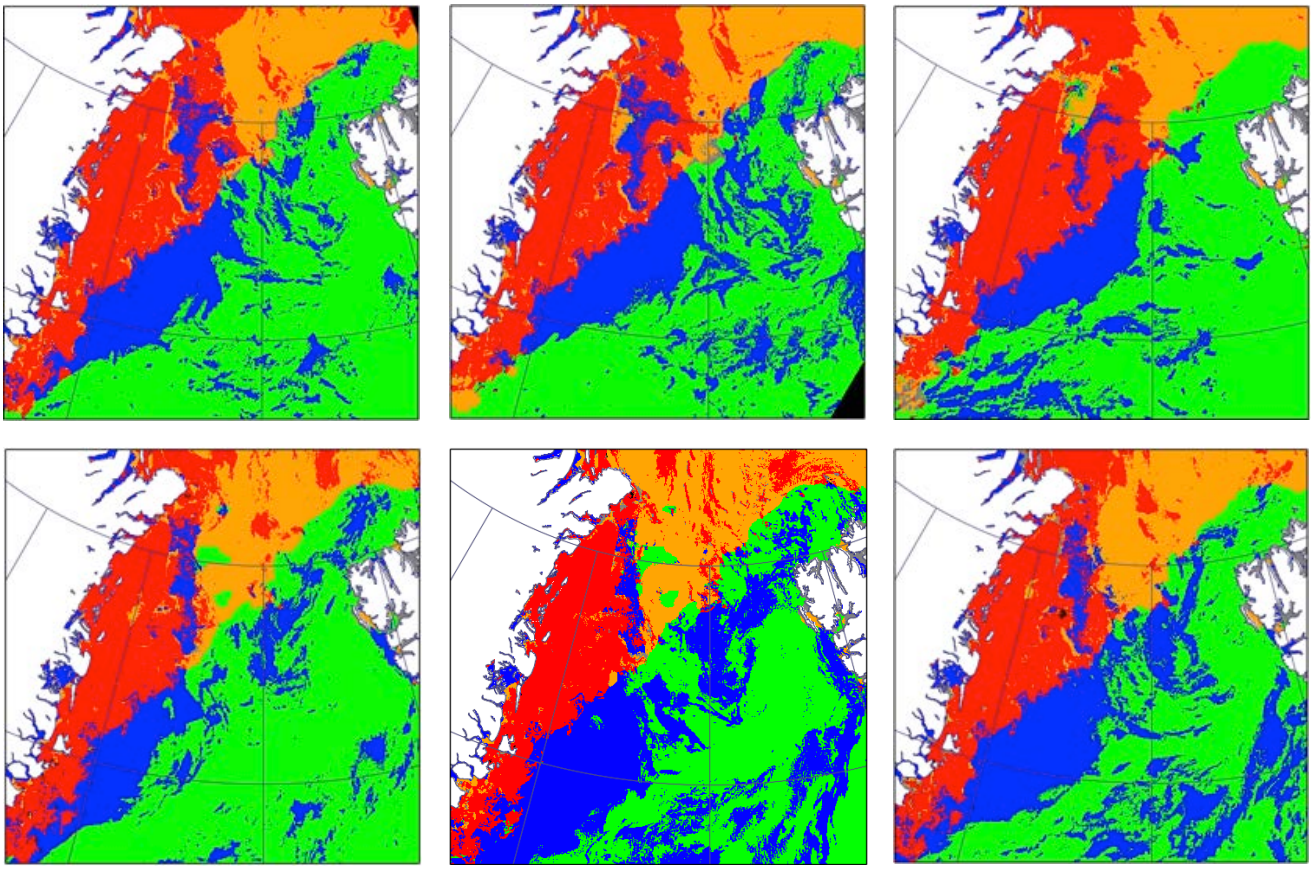

Figure 8. Labels, corresponding to overpasses shown in Figure 7. Land is rendered in white, ice in red, water in blue, clouds over water in green, clouds over ice in orange. Black pixels correspond to region not covered by the considered overpass.

After labeling for each overpass is completed, we can merge them to obtain a high-resolution daily ice extent product. Daily ice products can take advantage of cloud movement and multiple granules to provide more opportunities for un-occluded visible observations of the earth surface. When multiple visible observations of the same portions of the surface are available, individual granule products provide an opportunity to study ice changes or motion within a day. Combining the pre-labeled gridded scene overpasses can be done using logic that assigns higher weights to imager-based classification from Step 1 and lower weights to classification involving microwave observations obtained in the Steps 2 & 3.

4. EVALUATION

We have been evaluating the MISIC product since the summer of 2015. To make evaluations easier, we have developed the web-based monitoring system that allowed us to compare the performance of our algorithm with the several independent operational daily products. The list of products incorporated into the system includes the Interactive Multisensor Snow and Ice Mapping System (IMS) produced and hosted by the National Ice Center; the Daily Sea Ice Concentration Analyses product produced and hosted by the Marine Modeling & Analysis Branch (MMAB) of the National Centers for Environmental Protection (NCEP); the Global Sea Ice Concentration product produced and hosted by the Ocean and Sea Ice Centre at the EUMETSAT Network of Satellite Application Facilities (OSI SAF); and the Global Daily Ice Edge product produced by the Canadian Meteorological Center (CMC) and distributed by the NASA Jet Propulsion Laboratory through the Physical Oceanography Distributed Active Archive Center (PODAAC).

The system provides gridded images for a selected region of interest on a user specified date. For each satellite observation at the granule level, these images will include a true color RGB, our proposed false color and ice extent, and the current operational VIIRS ice fraction product with the ability to navigate between different overpasses.

The system was developed using the Python scientific stack for the image generation. The frontend was developed using HTML5 technology (Javascript, CSS and HTML.) The frontend development uses the popular and well-supported Zurb Foundation, as well as SASS. JSON is used for data serialization.

Figure 9 shows a screen capture of our monitoring system with the following selections: Beaufort Sea, VIIRS (6th overpass), False Color, July 13, 2016. The overpasses are saved in the UTC order and with the mouse position over the image, the full granule name is displayed. Download options are GeoTiff and PNG.

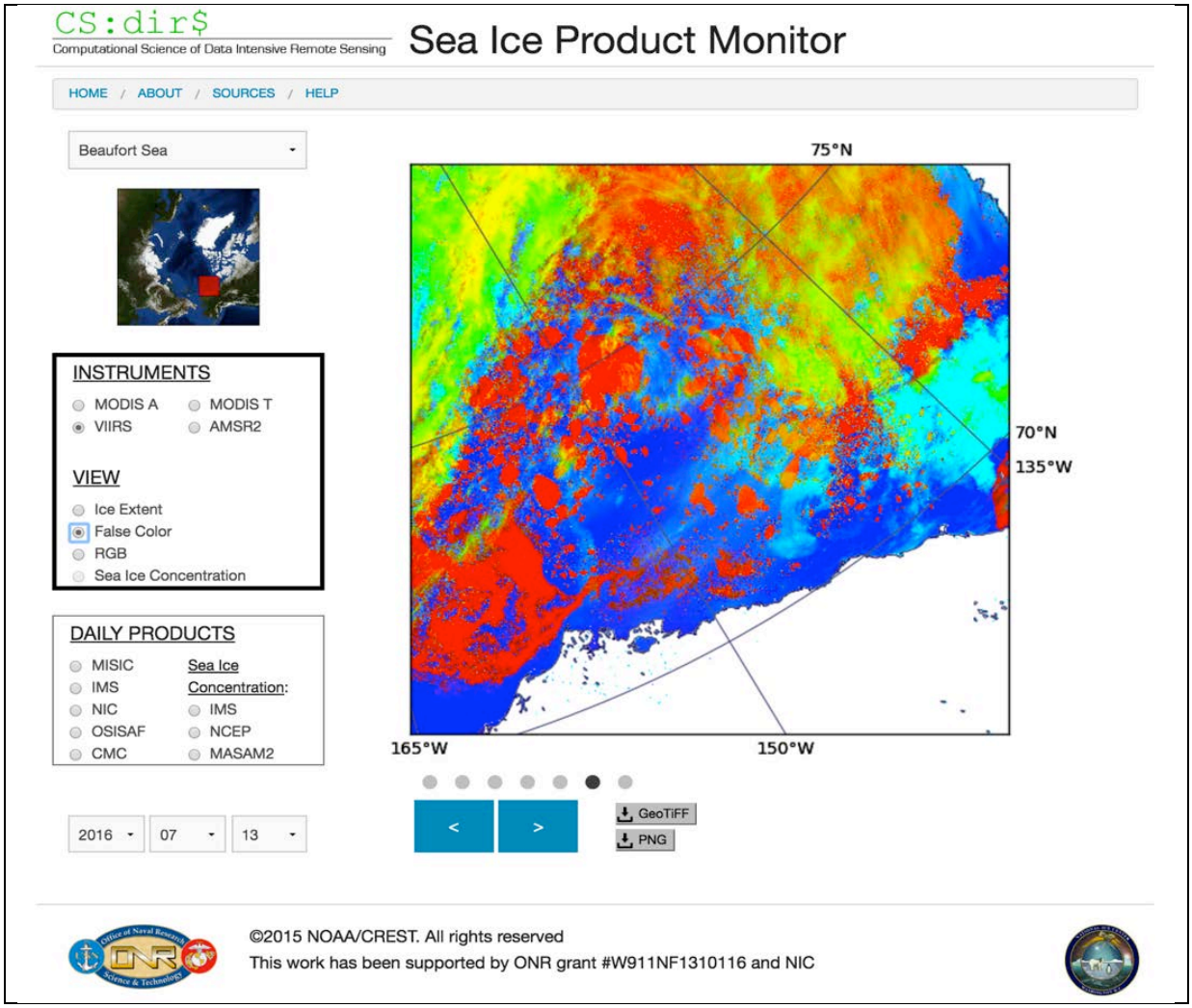

Figure 9: Screen capture of the current state of web-based monitoring system

5. CONCLUSION

We have developed and implemented an automatic algorithm, MISIC, capable of using imager and microwave data from multiple instruments (MODIS, VIIRS, and AMSER-2) to estimate sea ice cover. The algorithm produces a single-pass enhanced version, which combines the data from an imager single-pass with microwave data. We also show how to use multiple passes to create daily product consistent with state of the art interactive products produced through expert guidance. Unlike approaches which simply use courser resolution microwave when clouds are present, our algorithm extracts surface information through thin and moderate clouds preserving information available in high resolution optical imagers whenever possible. Beyond direct use of the automated product, the derived I-W false color images can provide important guides since they quickly summarize many information sources and can thus to accelerate the creation of expert derived interactive products. Our sea ice product, algorithm and code (implemented in Python) is currently being evaluated by the Navy/NOAA National Ice Center (NIC) to assist in NIC products.

6. ACKNOWLEDGMENT

This work has been supported by ONR grant # W911NF1310116. We would like to thank program manager, Martin Jeffery, for constructive discussions and suggestions. We also would like to thank NIC analysts for marked up images and feedback on the algorithm performance.

REFERENCES

[1] Jin, Z.; Stamnes, K., Weeks, W.F., " The effect of sea ice on the solar energy budget in the atmosphere-sea ice-ocean system: A model study," Journal of Geophysical Research 99, 25281–25294 (1994).

[2] Vinnikov, K., Robock, A., Stouffer, R. J., Walsh, J. E., Parkinson, C.L., Cavalieri, D.J., Mitchell, J. F., Garrett, J., Zakharov, V. F., " Global Warming and Northern Hemisphere Sea Ice Extent," Science 286, 1934-1937 (1999).

[3] Serreze, M.C., Stroeve, J., "Arctic sea ice trends, variability and implications for seasonal ice forecasting.," Philosophical Transactions of the Royal Society A: Mathematical, Physical and Engineering Sciences 2045(373), 20140159-20140159 (2015).

[4] Parkinson, C.L., Cavalieri, D.J., "Antarctic sea ice variability and trends, 1979–2010," Cryosphere 6, 871-880 (2012).

[5] Liu, Y., Key, J., Wang, X., "Influence of changes in sea ice concentration and cloud cover on recent arctic surface temperature trends, " Geophys. Res. Lett. 36, (2009).

[6] Steele, M., Ermold, W., "Loitering of the retreating sea ice edge in the Arctic Seas," Journal of Geophysical Research (120), 7699–7721 (2015).

[7] Barry, R. G., "The Role of Snow and Ice in the Global Climate System: A Review," *Polar Geography* (26), 235-246 (2002).

[8] Pohl, C., Van Genderen, J. L., "Multisensor image fusion in remote sensing: Concepts, methods and applications," International Journal of Remote Sensing (19), 823-854 (1998).

[9] Ramsay, B. H., "The interactive multisensor snow and ice mapping system," Hydrological Processes (12), 1537–1546 (1998).

[10] Ramsay, B. H., "Prospects for the interactive multisensor snow and ice mapping system (IMS)," Proceedings of the 57th Eastern Snow Conference, 161-170 (2000).

[11] Helfrich, S. R., McNamara, D., Ramsay, B. H., Baldwin, T., Kasheta, T., "Enhancements to, and forthcoming developments in the Interactive Multisensor Snow and Ice Mapping System (IMS)," Hydrol. Process. (21), 1576–1586 (2007).